Synthesis, Molecular Characterization, and Biological Activity of Novel Synthetic Derivatives of Chromen-4-one in Human Cancer Cells

Vivek Barve,[†,‡] Fakhara Ahmed,[‡,§] Shreelekha Adsule,[§] Sanjeev Banerjee,[§] Sudhir Kulkarni,[||] Prashant Katiyar,[||] Christopher E. Anson,[⊥] Annie K. Powell,[⊥] Subhash Padhye,[†,§] and Fazlul H. Sarkar*[,§]

Department of Chemistry, University of Pune, Pune 411007, India, Department of Pathology, Barbara Ann Karmanos Cancer Institute, Wayne State University School of Medicine, 9374 Scott Hall, 540 East Canfield Avenue, Detroit, Michigan 48201, Vlife Science Technologies Pvt Ltd., 1 Akshay Residency, Plot No. 50 Anand Park, Aundh Pune 411007, India, and Institute for Inorganic Chemistry, University of Karlsruhe, D-76128 Karlsruhe, Germany

Received October 21, 2005

The synthesis and characterization of Schiff base derivatives of 3-formylchromone **3**−**6** (FPA-120 to FPA-123), the minimal biologically active structural motif of soy isoflavone, genistein, and their copper(II) complexes **7**−**10** (FPA-124 to FPA-127) are reported here. These copper complexes possess distorted square-planar geometries capable of stabilizing Cu^{2+}/Cu^{+} redox forms. The molecular modeling study revealed that the key interaction of the metal complexes was with amino acids in the pleckstrin homology (PH) and the kinase domain of the PKB (Akt) protein. Copper complex **7** significantly forms stronger charge interactions in the kinase domain than genistein, leading to better stabilization in the active pocket. In vitro evaluation of copper complexes against hormone-independent and metastatic breast (BT20), prostate (PC-3), and K-ras mutant (COLO 357) and K-ras wild-type (BxPC-3) pancreatic cancer cells revealed that **7** was the most potent compound which exhibited PKB (Akt protein) inhibitory activities and caused NF-κB inactivation in a well-established orthotopic pancreatic tumor model using COLO 357 cells. An inverse relationship was observed between IC_{50} values of the anti-proliferative activities and the Cu^{2+}/Cu^{+} redox couple for these compounds, which may provide a rapid screen for evaluating the efficacy of active metallodrugs affecting redox-senstitive transcription factors such as NF-κB and its upstream target, the PKB (Akt) pathway, in multiple cancers.

Introduction

Among the flavonoids and isoflavonoids found in plants with potential beneficial effects to human health, genistein (**1**), a major metabolite of soy, is believed to be one of the most potent anticancer agents.[1,2] Studies from our laboratory and others have found that genistein can inhibit the growth of various cancer cell lines, including leukemia, lymphoma, prostate, breast, lung, and head and neck, both in vitro and in vivo.[3−10] The compound has been shown to inhibit growth of cancer cells through modulation of genes that are related to the homeostatic control of the cell cycle and apoptosis.[11−13] It was also found that genistein could inhibit the activation of nuclear transcription factor, NF-κB,[14] and Akt signaling pathways,[15] both of which are known to maintain a balance between cell survival and programmed cell death (apoptosis). The structure−activity correlations for the isoflavonoid compounds have indicated certain features desirable for the antitumor properties of these compounds which include a chromone motif, with a double bond between C2−C3 positions and a side chain containing a phenyl ring having metal chelating ability.[16−18] These structural requirements can be easily built into the compound 3-formylchromone (**2**), which is a versatile synthon in heterocyclic chemistry, having antiinflammatory and anticancer activities, by condensing it with various amines in alcoholic medium, yielding corresponding Schiff bases. Such compounds are capable of forming metal complexes with several transition metal ions among which copper is particularly effective in yielding moieties with potent radical scavenging properties.[19]

The antiproliferative properties of genistein have been thought to be partly due to its strong antioxidant property for which they may enlist the help of relevant metal ions present in the biological system.[20−25] Chelation of metal ions has been shown to enhance antitumor effects via several different intracellular mechanisms.[26,27] For example, iron chelators have been shown to induce apoptosis through a p53-independent pathway[28] and by the inhibition of N-myc expression.[29] Similarly copper chelators induce apoptosis of tumor cells through inhibition of the NF-κB signaling cascade.[30] However, despite many of the active antitumor flavonoid or isoflavonoid compounds being effective metal ion chelators,[23,24] there have not been many studies on the metal complexes of biologically active isoflavonoids and their correlation with antioxidant potentials or their effects on the NF-κB signaling pathway.

In the present paper, we describe synthesis and characterization of four Schiff base derivatives of **2**. Conjugation with copper ions by these derivatives yields compounds with enhanced antiproliferative activities against hormone-independent BT20 and PC-3 cells as well as COLO 357 (K-ras mutant) and BxPC-3 (K-ras wild type) pancreatic cancer cell lines with IC_{50} values in therapeutically achievable concentration ranges. The fluorescence polarization method for the detection of serine/threonine kinase activity showed that **7** had the lowest IC_{50} in comparison with the other copper complexes in this series. Moreover, we report in vivo results on the most active compounds of this series, viz., **7**, in an established orthotopic

* To whom correspondence should be addressed at the Department of Pathology, Karmanos Cancer Institute, Wayne State University School of Medicine, 715 Hudson Webber Cancer Research Center, 110 E. Warren, Detroit, MI 48201. Phone: 313-576-8327. Fax: 313-576-8389. E-mail: fsarkar@med.wayne.edu.

[†] University of Pune.

[‡] V.A. and F.A. have contributed equally to this work.

[§] Wayne State University.

[||] Vlife Science Technologies Pvt Ltd.

[⊥] University of Karlsruhe.

10.1021/jm051068y CCC: $33.50
Published on Web 06/03/2006

Scheme 1. Schematic Structures of Genistein (**1**) and 3-Formylchromone (**2**), Its Schiff Bases **3**−**6**, and Its Metal Complexes **7**−**10**

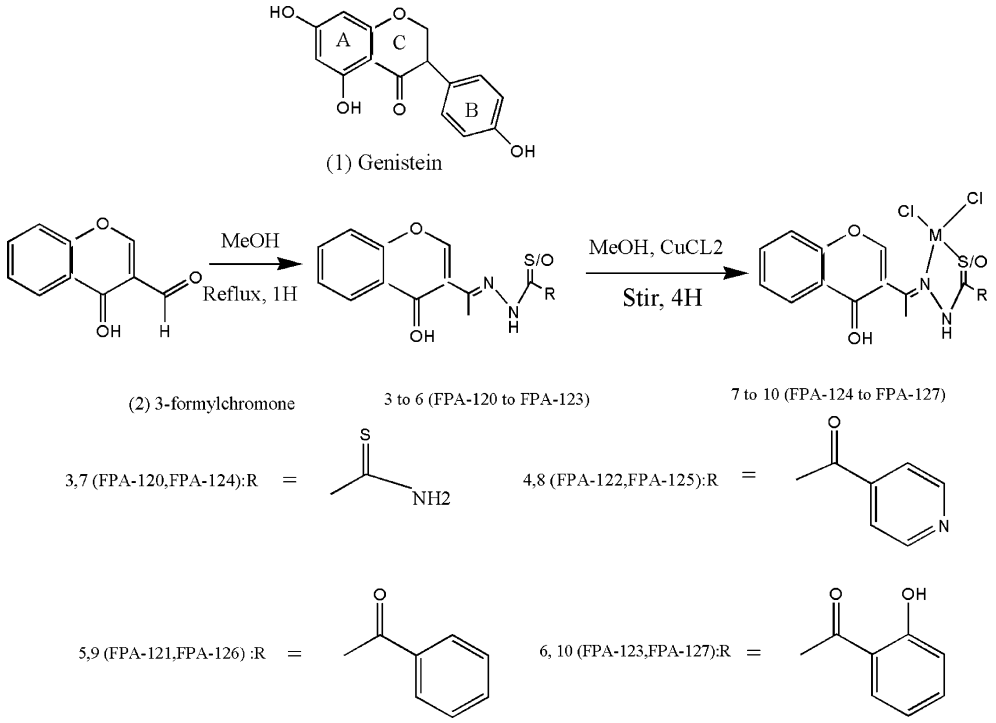

animal model of pancreatic cancer showing that this compound down-regulates the nuclear transcription factor NF-κB, which is known to be regulated by the PKB (Akt) protein and is responsible for rendering resistance against many cancer chemotherapeutic agents. Our present results suggest that carefully designed metal complexes of genistein analogues may provide useful chemotherapeutic agents for the treatment of, at least, three of the most common human cancers.

Results and Discussion

The Schiff base ligands **3**−**6** (Scheme 1) were synthesized by condensing equimolar amounts of **2** with various amines in methanolic solvent and recrystallizing the resulting compounds from dimethylformamide (DMF)−methanol (1:1) solvent. The ligands were interacted further with copper chloride in the stoichiometric ratio to precipitate out the corresponding metal complexes **7**−**10**, which were purified by the chromatographic workups. The selected amines are effective pharmacophores found in many therapeutic compounds currently used in the clinical practice and serve as spacers in the present design, keeping the cytotoxic metal complexes away from the isoflavonoid moiety. Such a strategy was found to be useful for retaining pharmacological properties of both the carrier and cytotoxic moieties.[31]

The ^{1}H NMR spectra of ligands **3**−**6** were recorded in dimethyl sulfoxide-d_6 (DMSO-d_6) on a Varian-Mercury 300 MHz spectrometer using $Si(CH_3)_4$ as an internal standard. The ^{1}H NMR spectra of ligands **3**−**6** in DMSO-d_6 exhibits signal in the region of 11−12 ppm, which can be attributed to the amide proton and confirms the *E*-isomeric form.[32,33] The presence of a downfield NH proton for them may be due to the involvement of this group in the hydrogen bonding with DMSO-d_6, which is well-known for the amide proton.[34] The downfield shift of the −OH proton in **6** that resonates at 11.80 ppm indicates that the −OH proton in this ligand is probably involved in the formation of strong intramolecular hydrogen bonding.[35] Thus, ^{1}H NMR spectra of ligands **3**−**6** displaying signals corresponding to the −NH and −OH protons confirm the existence of the keto form and the absence of deprotonation in these compounds. The aromatic protons appear in the range of 6−8.2 ppm for all compounds.[36] Compound **3** contains an isothiocyanate function (although not terminal as in sulforaphanes), which has been shown to be capable of activating MAPKs, NRF, ARE-mediated luciferase reporter genes and phase II enzyme gene induction.[37,38]

The spectroscopic data indicate that, during metal conjugation, ligands **3**−**6** behave as bidentate thionic moieties coordinating through azomethine nitrogen and thiocarbonyl sulfur/enolic hydroxyl (in the case of hydrazonates), respectively. The electronic spectra confirm the square-planar geometries for the copper complexes with the presence of $^2B_{1g} \rightarrow {}^2A_{1g}$ and $^2B_{1g} \rightarrow {}^2E_g$ transitions, respectively.[39,40] The absorption at 25 000 cm^{-1} observed for compound **7** is ascribed to the S → Cu(II) charge-transfer band,[41] while the absorption in the region of 22 000−24 000 cm^{-1} is due to an oxygen to copper charge-transfer transition.[42] The magnetic moments of the copper compounds (1.74−1.94 μ_B) are typical of monomeric compounds having distorted square-planar geometries.[43] The electron paramagnetic resonance (EPR) parameters further confirm such geometries with a parametric relation $g_{\|} > g_{\perp} > 2.0$ and $A_{\|}$ values around 175−140 G.[44] The distortion factor f (given by $g_{\|}/A_{\|}$) calculated for the present compounds are comparable with analogous copper complexes reported in the literature.[45] This parameter has been suggested to be important for designing copper compounds having radical scavenging properties.[46]

The electrochemical profile of **3** (Supporting Information) indicates an irreversible reduction peak centered at −1.30 V which is due to the reduction of the azomethine (C═N) function.[47] A similar peak is also observed in the case of compounds **3**−**6**. An additional quasireversible peak at −0.65 V is assigned to the reduction of the aroylhydrazone moiety in the case of the hydrazonate ligands. We calculated the redox reversibility for all copper complexes, and these are shown in Table 1 on page 9 of the Supporting Information. The i_{pa}/i_{pc}

ratio for all copper complexes falls in the range of 0.75−0.95, indicating that the couples are 75−95% reversible. To confirm this, we also carried out the scan rate dependence of all the copper complexes using cyclic voltammetric methods, and this shows that the redox peaks observed for **7** (FPA-124) are indeed reversible as compared to the parent ligand **3** (FPA-120), which does not show any redox peak (Figure 1c in the Supporting Information on page 6).

All copper complexes show a reversible Cu(II)/Cu(I) redox couple in the range of +0.28 to +0.35 V, indicating a facile reduction of the cupric center. One of the properties of the metal complexes is increased liposolubility. This increases the ability of the drug molecules in crossing the cell membrane, thus increasing the biological availability and hence its activity. Our result suggests that the structure and conformation of the ligand has influence on the redox potential of the central atom of the coordination compound. This is observed with the present isoflavone derivatives **3**−**6,** where changes in the coordination sphere are connected with the change of biofunction of compounds, as shown in Figure 4.

Previously, 3′,4′-*O*-substituted derivatives of isoflavones have been developed as therapeutic agents against protein tyrosine kinase (PTK) and molecular modeling studies have confirmed that isoflavonoids have the structural features important for binding to SH2 domain of p56lck protein kinase.[48] The PDB structure of the PH domain of the human protein kinase B-α isoform was available in protein databank (PDB code: 1UNP).[49] However, the X-ray crystal structure for the kinase domain of the PKBα isoform was not available in the protein databank. To investigate the interactions of the parent genistein and the metal complex **7** with the active domains of the PKB (Akt) protein, namely, PH and the catalytic kinase domain, we carried out homology modeling studies for **7** using the program VLifeMDS 2.0 (VLifeMDS 2.0, Molecular Design Suite developed by VLife Sciences technologies Pvt Ltd.)[50] in order to obtain a model for the kinase domain of PKBα by using X-ray crystal structure of PKB*β* (PDB code: 1GZK, sequence identity 86% and similarity 94% with the α-isoform) as template.[51,52] The conformation analysis of genistein (**1**) and its complexes **7**−**10** was done by using the Monte Carlo conformation method, and conformers satisfying steric requirement of the each cavity were considered for docking.[53] The MMFF94 force field was utilized for energy minimization to a gradient root mean square (RMS) of 0.1 kcal/(mol·Å) in order to remove local structural defects such as steric hindrance and unusual bond lengths, bond angles, and torsions.[54,55] All the minimizations were carried out in the absence of water, assuming a dielectric constant (ϵ) equal to 1.The charge equilibrium Q_{eq} method provided the functions to calculate forces on atoms and energy of atoms and metals such as Cu^{2+} explicitly bonded to the other four atoms. We used certain parameters for selecting the conformers. After the ligands were placed in the active site, the residues were flexed within 10 Å, and residues beyond 10 Å were frozen. We chose this method because residues beyond 10 Å are unlikely to interact with the ligand. A second criterion used was based on the similarity between the force field and root-mean-square distance (RMSD) calculated over heavy atoms and polar atoms of the ligand conformers. Conformers with a difference in energy (based on the nature of potential energy) by at least 1 kcal/mol were chosen. The conformers were selected and placed in the active site, and the atoms of the ligand that form a ring with Cu^{2+} along with two chlorine atoms were aggregated and the resultant complex structures were energy-minimized to a gradient-RMS of 0.1 kcal/(mol·Å) using MMFF94 force-field in VLifeMDS 2.0. The binding energy was then calculated as

$$E_{binding} = E_{complex} - (E_{apo} + E_{ligand})$$

The kinase domain cavity is comprised of a buried hydrophobic interior and a relatively less buried hydrophilic surface. While the polar exposed portion of the cavity is characterized by the presence of charged residues such as glutamates (Glu274, Glu310), aspartates (Asp270, Asp288), and Thr156, the buried hydrophobic interior of the cavity is characterized by the presence of hydrophobic residues such as Phe289, Leu291, Leu152, Val160, and Ala173. Unlike the kinase domain, the PH domain ligand binding cavity is primarily shallow and hydrophilic in nature. The presence of an ample number of lysine and arginine residues such as Arg25, Arg23, Lys14, Arg86, Arg15, and Lys39 renders a positively charged nature to the cavity surface. However, one negatively charged residue, Glu17, is also present on the cavity surface, thereby conferring an acidic nature to a relatively smaller region of the cavity surface. It is worth noticing that the PH domain cavity lacks a hydrophobic buried interior as observed in the kinase domain. Hence, we believe that these fundamental differences, viz., electrostatics and shape−size characteristics of the kinase and PH domain, form the underlying basis for variable binding affinity as well as specificity of different ligands docked into these two domains.

It was observed that the aromatic chromone ring of genistein interacts with Arg25 and the phenolic −OH of the B-ring of genistein interacts with the carboxyl group of Glu17, leading to stabilization in the PH domain. Hydrophobic interactions were not found to contribute to genistein binding in any manner because of a lack of any significant hydrophobic residues in the PH domain cavity. Unlike genistein, metal complex **7** binding in the PH domain is stabilized by an additional hydrogen bond with key amino acids Arg25, Glu17, and Ile19 that are involved in the stabilization of the receptor−ligand complex (see the Supporting Information for docking figures). Since different PH domains normally share less than 20% sequence identity, this may facilitate the development of drugs that bind specifically to the PH domain of the PKB protein. It was observed that some charged residues such as Arg86, Asn53, and Lys14 are yet unexploited and provide an ideal opportunity for further modifications to the benzopyran motif, which may yield highly potent molecules with enhanced PKB inhibitory activity.

The crystal structure of the kinase domain of the PKB protein bound to AMP−PNP, which is an inhibitor analogous to natural substrate ATP, is reported in the literature (PDB ID: 1O6K). The AMP−PNP ligand does not directly bind to THR308 yet prevents its phosphorylation (see Supporting Information). It was seen that the genistein molecule interacts with the hydrophobic cavity of the the kinase domain of the PKB protein, where its single phenolic ring structure orients itself to hydrogen bond with the C═O of the Met223 and the −OH group of B ring binds to the carboxyl group of Glu274 (Figure 1a, where hydrogen bonds are shown in pink).

The docking studies of **7** have shown that the metal complex has three kinds of interactions with the receptor protein. The hydrophobic chromone end of **7** interacts with the hydrophobic interior of the cavity, namely, the hydrophobic side chains of the residues Phe289, Leu(291,152), and Val160. Second, there exists a hydrogen bond between the backbone N−H of Gly290 and the ethereal oxygen atom of **7**. As the copper atom carries a partial positive charge, the metal complex interacts with the

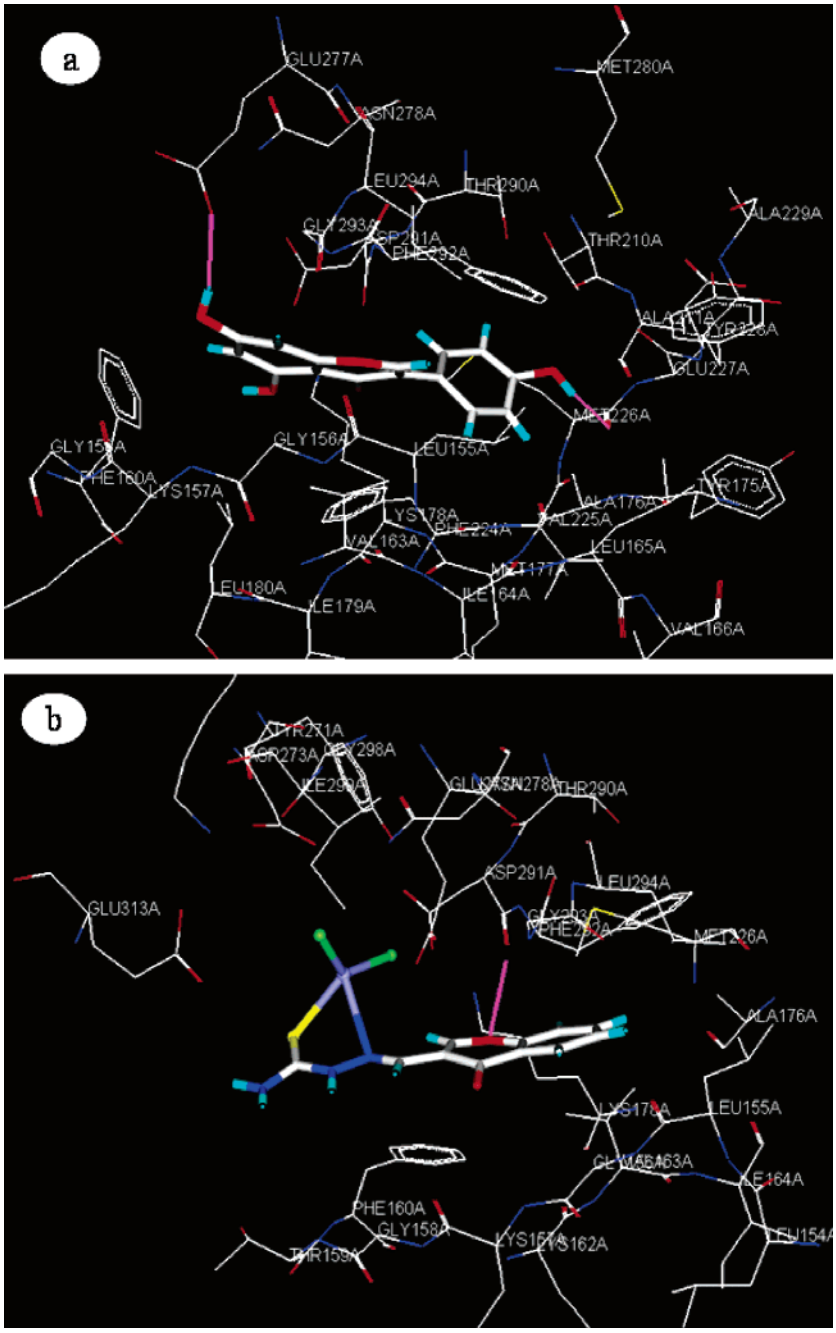

Figure 1. (a) Docking of genistein (**1**) into the kinase domain of the PKB (Akt) protein, showing the interactions within the hydrophobic cavity where the phenolic ring structure of genistein hydrogen bonds with C═O of the Met223 and the −OH group of B ring binds to the carboxyl group of Glu274 in the kinase domain of the PKB protein. (b) Key interactions of **7** with the active site of the kinase domain of the PKB protein, showing stronger charge interactions as well as hydrogen bonding with the N−H of Gly290, electrostatic interactions with carboxyl groups of Glu274, Glu310, Asp270, and Asp288 as well as hydrophobic interactions with residues Phe289, Leu(291,152), and Val160.

carboxyl groups of Glu274, Glu310, Asp270, and Asp288 through electrostatic interactions (Figure 1b). From these modeling experiments, we found that genistein had one extra hydrogen bond interaction over **7** with the PKB protein, whereas the **7** showed charge interactions within the kinase domain. Hence, we conclude that the metal complex **7** could lead to better stabilization because charge interactions are stronger than hydrogen bonding; it leads to better stabilization of the parent genistein, yielding higher potent kinase inhibitory activity as supported by our fluorescence polarization IC_{50} data (Table 1).

When we examined the biological effects of these compounds against the hormone-independent breast (BT20) and prostate (PC-3) cancers as well as K-ras mutant COLO 357) and K-ras wild-type (BxPC-3) pancreatic cancer cell lines, the metal complexes exhibited dose-dependent growth inhibitory effects

Table 1. IC_{50} Values of **7**, **8**, and **10** by MTT and Fluorescence Polarization Assay in BT20, PC-3, BxPC-3, and COLO 357 Cancer Cell Lines

	MTT cell proliferation assay IC_{50} (μM)				fluorescence polarization Akt kinase assay IC_{50} (μM)
Compounds	COLO357	BxPC3	BT20	PC3	
genistein	50	30	46−70	50	>70
7	34	55	7	10	0.1
8	30	20	12	15	15
10	16	22	12	14	8

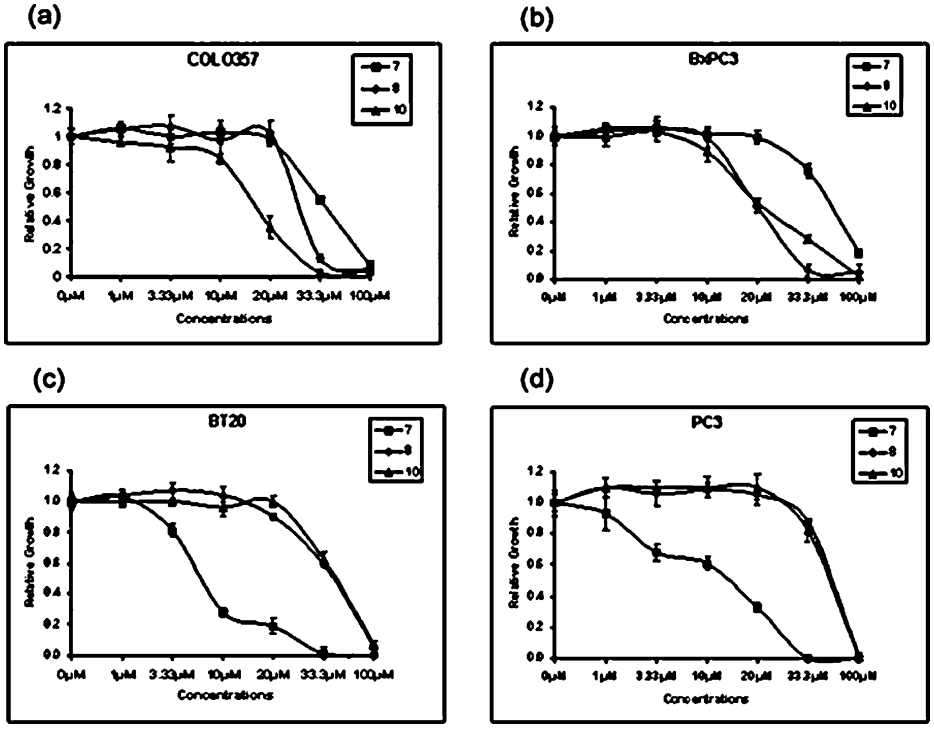

Figure 2. Inhibition of cell growth after treatment for 72 h with copper complexes **7**, **8**, and **10** on cancer cell lines: (a) K-ras mutant pancreatic COLO 357 cancer cells; (b) K-ras wild-type pancreatic BxPC-3 cancer cells; (c) estrogen-independent BT20 breast cancer; (d) androgen-independent PC-3 prostate cancer cells. (IC_{50} is defined as the concentration of the compound required to inhibit proliferation of cells by 50%.)

in all of the cell lines. Most importantly, **7**(FPA-124) showed 50% cell kill at concentrations of 7 μM in BT20 and 10 μM in PC-3 cells (Figure 2). The metal complexes **7**, **8**, and **10** inhibited growth of BxPC-3 and COLO 357 cells at concentration > 20 μM, whereas the metal complex **9** showed a cell kill in all of the four cell lines at very high doses (>50 μM). We observed a synergistic enhancement in the antiproliferative activities upon metal conjugation compared to their corresponding parent ligands **3**−**6** (Figure 5 on Supporting Information page 8) as well as to the parent genistein (positive control), which has IC_{50} values > 40 μM in these multiple cancer cell lines.

In our earlier work, it was observed that metal conjugation renders a pleiotrophic characteristic to the organic ligands which are essential for treating a heterogeneous disease like cancer.[56] Compounds with well-defined but singular targets have been found to have limited therapeutic value due to associated but unanticipated side effects and rapidly built resistance. On the other hand, metal complexes are able to assert effects on multitarget sites (whether in intact or dissociated configurations) and hence exhibit superior activity and comparatively less frequency of resistance. A comparison of the IC_{50} values of present metal complexes with those of genistein revealed substantial decrease indicating therapeutically achievable efficacy (Table 1). Since all copper compounds were redox active metal complexes, we believe that redox triggered oxidative stress may be one of the underlying mechanisms for the observed apoptotic cell death in the present case.

The quantitative evaluation of the apoptosis by ELISA for the metal complexes **7**, **8**, and **10** has been carried out in four cancer cell lines COLO 357, BxPC-3, BT20, and PC-3, respectively (Figure 3). It was observed that metal complexes **7**, **8**, and **10** induced apoptosis in the entire cancer cell lines tested and **7** showed the highest index of apoptotic cells in PC-3 cells. The bar graph in Figure 3 is the mean of three separate experiments carried out. This observation is also in accordance with the favorable distortion factor calculated for the present copper compounds using EPR spectra as suggested by Cao et al.,[46] which helps stabilize cuprous and cupric species without dissociation of the complex.

Interestingly, we observed an inverse relationship between the metal redox couple and the IC_{50} values for the present metal complexes against the hormone-independent breast and prostate cancer cell lines (Figure 4a,b). Further to show the correlation between E_o and liposolubilities, we calculated the log *P* values of the metal complexes **7**−**10** (FPA-124 to FPA-127). Our results show that although the copper complex FPA-124 has a lower log *P* than other complexes, a high positive redox value $E_{1/2}$ of the metal complex FPA-124 correlates with higher liposolubility and thus higher biological activity (inhibition of cell growth in vitro) as shown in Figure 4c.

We have calculated the stability constants of these copper complexes via Job's ratio method[57] (mole ratio method) as log $K = 4.10$, which confirms that these complexes are mildly stable at neutral pH. Various copper complexes have similar log *K* values which sustain their structures under physiological conditions as described previously.[58] These results are supported by our additional findings as shown in the scan-dependent experiments by cyclic voltammetry (Figure 1b,c on Supporting Information page 6). The intactness of the copper complexes during redox cycling of the copper center through the Cu^{2+}/Cu^{+} couple is also supported by the distortion factors (*F*) calculated for these compounds from their EPR spectra (average value = 150 G) (Supporting Information Table 2b on page 10). From our results it follows that the structure and conformation of the ligand has influence on the redox potential of the central atom in the coordination compound, indicating that this parameter can indeed be used as a guideline for developing effective antitumor metal complexes against these cancers.

In further experiments using fluorescence polarization-based assays,[59,60] we investigated whether the effects of the present metal complexes **7**, **8**, and **10** could be mediated by inactivation

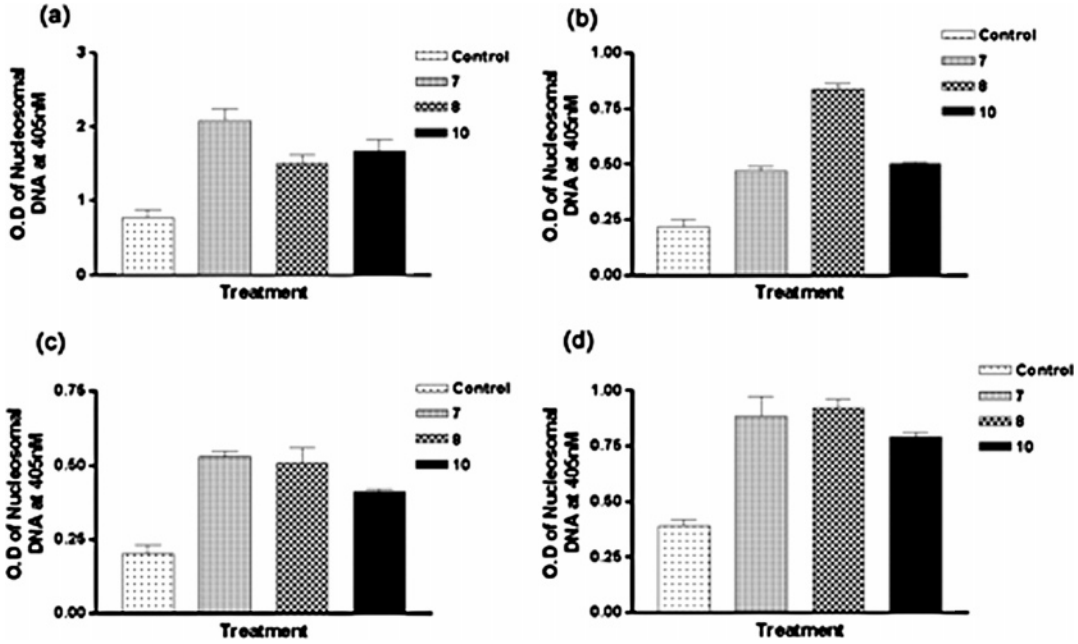

Figure 3. Induction of apoptosis in cancer cells by ELISA, showing data from (a) K-ras mutant pancreatic COLO 357 cancer cells, (b) K-ras wild-type pancreatic BxPC-3 cancer cells, (c) estrogen-independent BT20 breast cancer, and (d) androgen-independent PC-3 prostate cancer cells (control, 20 μM (**7**, **8**, and **10)** treated cells).

of serine/threonine kinase activity, since PKB (Akt) signaling is important in cancer development as it promotes cell survival by inhibiting apoptosis through inactivation of proapoptotic factors. The PKB (Akt) protein has been shown to influence many transcription factors that are involved in controlling the cell growth and survival such as E2F, NF-κB,[61] and CREB and are also known to cross-talk with the RAF/Erk signaling pathways.[62] The PKB (Akt) protein is activated by phospholipid binding and phosphorylation at Thr308 by PDK1 or Ser473 by PDK2, respectively.

The IC_{50} values of our compounds are presented in Table 1. Compound **7** exhibited the lowest IC_{50} value compared to other copper complexes in inhibiting Akt kinase activity. It is interesting to note that the Akt kinase activity could be inhibited with 100 nM (IC_{50}) of **7** but the IC_{50} for inhibiting cell growth is 70−100-fold greater than the inhibition of kinase activity. Further studies are underway to understand these results.

Activation of NF-κB in cancer cells has been shown to attenuate apoptosis induced by chemotherapeutic agents resulting in lower cell killing and drug resistance. Since the NF-κB pathway is regulated by Akt protein, we decided to investigate the effects of the lead copper complex of the present series, **7**, on the NF-κB activity through an in vivo experiment in a well-established orthotropic pancreatic tumor model using COLO 357 cells.[63] The parent genistein compound has been shown to inhibit the activity of NF-κB and the growth of hormone-dependent (LNCaP) and hormone-independent (PC-3) human prostate cancer cell lines in vivo without causing systemic toxicity.[64] Recently, we have also observed potentiating effects of genistein leading to inhibition of tumor growth by radiation in a prostate cancer orthotopic model[65] and the effect of chemotherapy in orthotopic pancreatic cancer model.[66] In this study, our results showed that **7** had no apparent animal toxicity, as indicated by no change in the body weight of the treated animals (Figure 5a) but caused a decrease in the tumor load (Figure 5b). Most importantly, the NF-κB activity was significantly decreased in **7**-treated animal tumor tissues, supporting the in vivo effect of **7** through the Akt/NF-κB pathway (Figure 5c).

In conclusion, the knowledge of the 3D structure of the biological target as well as the specialized computational software constitutes a powerful approach to design libraries of inhibitors with specific activity for PKB (Akt) protein. Our structure-based focused approach has led to the identification of bioactive thiosemicarbazonate or hydrazonate pharmacophores appended to the chromone motif capable of copper conjugation as novel antitumor molecules compared to genistein, which are capable of inhibiting NF-κB activation through the PKB (Akt) pathway in the animal model. Further work is ongoing in our laboratory to unravel the underlying mechanism of their superior cell killing action and the role played by cupric ions in these novel metal-based antitumor agents.

Experimental Section

Chemical Methods. Unless otherwise noted all solvents, chemicals, and reagents were obtained commercially and used without purification. The ^{1}H NMR spectra were carried out on a Varian-Mercury 300 Hz spectrophotometer using $Si(CH_3)_4$ as an internal standard.

Synthesis of 3-Formylchromone Schiff Bases (3−6). The Schiff base ligands **3**−**6** (Scheme 1) were synthesized by mixing equimolar amounts of **2** with thiosemicarbazide hydrochloride (**3**), benzoyl hydrazide (**4**), isonicotinoyl hydrazide (**5**), and salicylic hydrazide (**6**), respectively, in methanolic solvent and maintaining the reaction mixture at reflux temperature for 1 h. The products obtained were filtered off, recrystallized from (1:1) DMF−methanol, and finally dried in a vacuum desiccator over anhydrous $CaCl_2$. ^{1}H NMR data for **3**−**6** are listed in the Supporting Information.

3-Formylchromone Thiosemicarbazone (3). ($C_{17}H_{10}N_2O_3$): C, 53.88%; H, 3.32%; N 16.50%; S, 12.76% (calcd: C, 53.44%; H, 3.64%; N, 17.00%; S, 12.95%).

3-Formylchromone Benzoyl Hydrazone (4). ($C_{16}H_9N_3O_3$): C, 69.86%; H, 4.10%; N 9.58% (calcd: C, 63.43%; H, 4.38%; N, 9.01%).

3-Formylchromone Isonicotinyl Hydrazone (5). ($C_{16}H_9N_3O_3$): C, 65.00%; H, 3.48%; N, 14.06% (calcd: C, 65.00%; H, 3.75%; N, 14.33%).

3-Formylchromone Salicylic Hydrazone (6). ($C_{17}H_{11}N_2O_4$): C, 65.68%; H, 3.89%; N 9.03% (calcd: C, 66.23%; H, 3.87%; N, 9.09%).

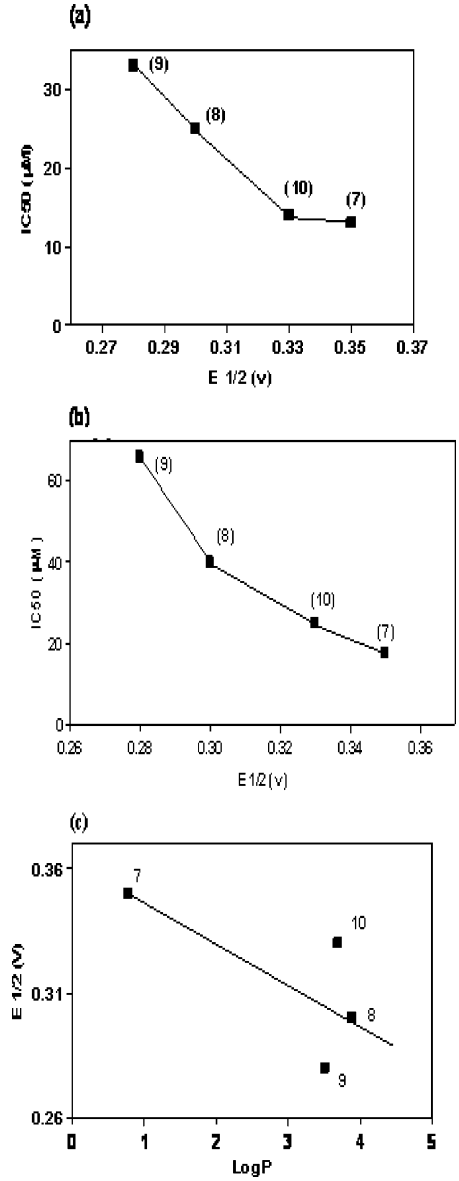

Figure 4. Plot showing correlation between IC_{50} (μM) values and the metal redox couple ($E_{1/2}$) for copper complexes **7**−**10**.

Synthesis of Metal Complexes (7−10). The copper(II) complexes of **7**−**10** were synthesized by mixing equimolar amounts of the ligands and $CuCl_2 \cdot 2H_2O$ in methanol with a trace amount of dimethylformamide. The resulting mixture was refluxed at room temperature for 1 h. The precipitates formed were removed by filtration, washed with the methanol solvent, and dried in a vacuum over anhydrous $CaCl_2$. The analytical elemental data for the copper complexes (**7**−**10**) of 3-formylchromome are given in the Supporting Information.

Biology. Akt Kinase Assay by Fluorescence Polarization. Serine/threonine Akt kinase reaction was carried out in 96-well black plates in a total volume of 100 μL using a Ser/Thr kinase polarization based assay kit from Invitrogen Part No. P310353. The Akt kinase assay was done in vitro using fluoroscence polarization based on the following principle. Briefly, enzyme is incubated with the substrate in the presence of ATP and ideal buffer conditions. In the absence of enzyme inhibitor, complete enzymatic reaction takes place, resulting in the production of a maximum amount of phosphopeptide, while in the presence of enzyme inhibitor it blocks the reaction, resulting in the reduction of phosphopeptide product. This phosphopeptide competes with fluorescently tagged phosphopeptide for its binding to the anti-phospho antibody in the assay plate. Therefore, the availability of a greater amount of unlabeled phosphopeptide in the reaction results in a lesser amount of fluorescent phosphopeptide available for binding to antibody, thereby causing less polarization, which reflects higher Akt kinase activity. On the other hand with fewer unlabeled phosphopeptides due to Akt kinase inhibition, more fluorescent phosphopeptide will bind to the antibody, resulting in a higher polarization value, which reflects the inhibition of the Akt kinase activity.

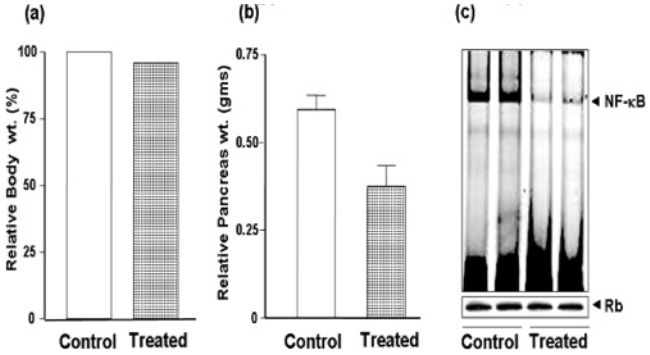

Figure 5. Data representing an average of two independent experiments with a total of nine animals in each group. In vivo data showing (a) the relative body weight of control vs treated animals (treatment with **7** (25 mg/kg) body weight per mouse) (%), (b) the relative pancreas weight (%) of primary pancreatic tumors harvested from control versus treated mice with **7**, and (c) the gel shift assay showing down-regulation of NF-κB DNA binding activity in primary pancreatic tumors from two representative mice derived from control and treated groups.

For specific assays, the Akt kinase assay reaction was set up in a total volume of 40 μL in the presence of different concentrations of inhibitor. Stock solutions of test compounds were made in DMSO. From DMSO stocks, 4× solutions of compounds **7**, **8**, and **10** were prepared in 1× assay dilution buffer; 10 μL of the respective drug solution was used in the assay. Each reaction well had 25 ng of Akt1/PKBα, active enzyme (Upstate Biotechnology Catalog No. 14-276), 0.4 mM GSK-3 peptide (custom synthesized), ATP (100 μM) from Sigma Catalog No. A5394, and the test compound to be tested. A plate was incubated at 30 °C for 30 min. The enzyme reaction was quenched with 10 μL of 50 mM ethylenediaminetetraacetic acid (EDTA) for 5 min. Antiphosphoserine antibody was added at 25 μL/well followed by 10 μL of fluorescent tracer.

The total volume was made up to 100 μL by adding 15 μL of fluorescence polarization assay dilution buffer. Appropriate controls and blanks were prepared. The plate was incubated for 1 h at room temperature and was analyzed for polarization at 435 nm excitation and 535 nm emission wavelength on the Tecan Ultra microplate reader. Polarization values were normalized to the control and were plotted against the log concentration of the test compounds in Graph Pad Prism software. Sigmoidal dose response curve analysis was used to calculate the IC_{50} of the test compounds.

In Vivo Studies. Experimental Animals. Female nude mice (ICR−SCID) were purchased from Taconic Farms (Germantown, NY). The mice were housed and maintained under sterile conditions in facilities accredited by the American Association for the Accreditation of Laboratory Animal Care and in accordance with current regulations and standards of the United States Department of Agriculture, United States Department of Health and Human Services, and the National Institutes of Health (NIH). The mice were used in accordance with Animal Care and User Guidelines of Wayne State University under a protocol approved by the Institutional Animal Care and Use Committee. The mice received Lab Diet 5021 (Purina Mills, Inc., Richmond, IN).

Orthotopic Implantation of Tumor cells. COLO 357 cells were harvested from subconfluent cultures after a brief exposure to 0.25% trypsin and 0.2% EDTA. Trypsinization was stopped with medium containing 10% fetal bovine serum (FBS). The cells were washed once in serum-free medium and resuspended in phosphate buffer saline (PBS). Only suspensions consisting of single cells with >90% viability were used for the injections. The pancreas of anaesthetized

mice was exposed through a midline laparotomy incision and by retraction of the spleen. 2×10^5 cells in 20 μL PBS were injected into the parenchyma of the pancreas with a 27 gauge hypodermic needle and a Hamilton syringe as previously described by our laboratory.[65] The abdominal wound was sutured using a 5.0 chromic gut suture in a running fashion. On the basis of our previous experience with this model, we found a tumor take rate approaching >90%.

Mice were randomized into two treatment groups ($n = 9$, in each group): (a) untreated control; (b) **7**-treated (25 mg/kg, body weight) once every alternate day by intravenous (iv) injection (total of six injections). All mice were sacrificed on day 10 following the last dose of treatment, and their body weight was determined. The pancreas from all animals were excised and weighed. For routine H&E staining, one part of the tissue was fixed in formalin and embedded in paraffin and another part was rapidly frozen in liquid nitrogen and stored at −70 °C. H&E staining confirmed the presence of tumor(s) in each pancreas (data not shown).

Tumor Tissue Nuclear Protein Extraction and Electrophoretic Mobility Shift Assay (EMSA). Nuclear proteins were extracted from the tumor tissue as described previously.[66] The supernatant (nuclear proteins) was collected and kept at −70 °C until use. Protein concentration was determined using the bicinchonic acid assay kit with BSA as the standard (Pierce Chemical Co., Rockford, IL). The electrophoretic mobility shift assay (EMSA) was performed by incubating 8 μg of nuclear proteins with IR DyeTM-700 labeled NF-κB oligonucleotide. The incubation mixture included 2 μg of poly(dI−dC) in a binding buffer. The DNA−protein complex formed was separated from free oligonucleotide on 8.0% native polyacralyamide gel using buffer containing 50 mM Tris, 200 mM glycine, pH 8.5, and 1 mM EDTA and then visualized by Odyssey infrared imaging system using Odyssey software release 1.1.

Acknowledgment. S.A. gratefully thanks Dr. Jayendra Patole for the NMR data.

Supporting Information Available: Full experimental information for Schiff base isoflavone derivatives **3**−**6** and the metal complexes **7**−**10**, analytical characterization, and biological experimental assays. This material is available free of charge via the Internet at http://pubs.acs.org.

References

(1) Knight, D. C.; Eden, J. A. A review of the clinical effects of phytoestrogens. *Obstet. Gynecol. (N.Y.)* **1996**, *87*, 897−904.
(2) Mills, R.; Beeson, W.; Phillips, R.; Fraser, G. Cohort study of diet, lifestyle and prostate cancer in Adventist men. *Cancer* **1989**, *64*, 598−604.
(3) Davis, J. N.; Singh, B.; Bhuiyan, M.; Sarkar, F. H. Genistein-induced upregulation of p21^{WAF1}, down regulation of cyclin B and induction of apoptosis in prostate cancer cells. *Nutr. Cancer* **1998**, *32*, 123−131.
(4) Pagliacci, M. C.; Smacchia, M.; Migliorati, G.; Grignani, F.; Riccardi, C.; Nicoletti, I. Growth-inhibitory effects of the natural phytoestrogen genistein in MCF-7 human breast cancer cells. *Eur. J. Cancer* **1994**, *30A*, 1675−1682.
(5) Kyle, E.; Neckers, L.; Takimoto, C.; Curt, G.; Bergan, R. Genistein induced apoptosis of prostate cancer cells is preceded by a specific decrease in focal adhesion kinase activity. *Mol. Pharmacol.* **1997**, *51*, 193−200.
(6) Constantinou, A.; Huberman, E. Genistein as an inducer of tumor cell differentiation: Possible mechanisms of action. *Proc. Soc. Exp. Biol. Med.* **1995**, *208*, 109−115.
(7) Spinozzi, F.; Pagliacci, M. C.; Migliorati, G.; et al. The natural tyrosine kinase inhibitor genistein produces cell cycle arrest and apoptosis in Jurkat T-leukemia cells. *Leuk. Res.* **1994**, *18*, 431−439.
(8) Li, Y.; Upadhyaya, S.; Bhuiyan, M.; Sarkar, F. H. Induction of apoptosis in breast cancer cells MDA-MB-231 by genistein. *Oncogene* **1999**, *18*, 3166−3172.
(9) Li, Y.; Bhuiyan, M.; Sarkar, F. H. Induction of apoptosis and inhibition of c-erbB-2 in MDA-MB-435 cells by genistein. *Int. J. Oncol.* **1999**, *15*, 525−533.
(10) Alhasan, S. A.; Pietrasczkiwicz, H.; Alonso, M. D.; Ensley, J.; Sarkar, F. H. Genistein-induced cell cycle arrest and apoptosis in a head and neck squamous cell carcinoma cell line. *Nutr. Cancer* **1999**, *34*, 12−19.
(11) Barnes, S. Effect of genistein on in vitro and in vivo models. *J. Nutr.* **1995**, *125*, 7777−7835.
(12) Lian, F.; Bhuiyan, M.; Li, Y.; Wall, N.; Kraut, M.; Sarkar, F. Genistein induced G2M arrest, p21^{WAF1} upregulation and apoptosis in a NSCL cancer cell line. *Nutr. Cancer* **1998**, *31*, 184−193.
(13) Upadhyaya, S.; Neburi, M.; Chinni, S.; Alhasan, S.; Miller, F.; Sarkar, F. Differntial sensitivity of normal and malignant breast epithelial cells to genistein is partly mediated by p21^{waf1}. *Clin. Cancer Res.* **2001**, *7*, 1782−1789.
(14) Davis, J. N.; Kucuk, O.; Sarkar, F. H. Genistein inhibits NF-κB activation in prostate cancer cells. *Nutr. Cancer* **1999**, *35*, 167−174.
(15) Li, Y.; Sarkar, F. H. Inhibition of nuclear factor kB activation in PC-3 cells by genistein is mediated via Akt signaling pathway. *Clin. Cancer Res.* **2002**, *8*, 2369−2377.
(16) Bors, W.; Heller, W.; Michel, C.; Saran, M. Flavanoids as antioxidants: determination of radical scavenging efficiences. *Methods Enzymol.* **1990**, *186*, 343−355.
(17) Jovanvic, S. V.; Steenken, S.; Hara Y.; Simic, M. G. Reduction potentials of flavonoid and model phenoxyl radicals. Which ring in flavonoids is responsible for antioxidant activity? *J. Chem. Soc., Perkin. Trans.* **1996**, *2*, 2497−2504.
(18) Rice-Evanas, C. A.; Miller, N. J.; Paganya, G. Structure-antioxidant activity relationships of flavonoids and phenolic acids. *Free. Radical Biol. Med.* **1996**, *20*, 933−956.
(19) Patole, J.; Dutta, S.; Padhye, S.; Sinn, E. Tuning up SOD activity of salicylaldehyde semicarbazone by heterocyclic bases. *Inorg. Chim. Acta* **2001**, *318*, 207−211.
(20) Ishige, K.; Scalese, M.; Sagara, Y. Flavonoids protect neuronal cells from oxidative stress by three distinct mechanisms. *Free Radical Biol. Med.* **2001**, *30*, 433−446.
(21) Saija, A.; Scalese, M.; Lanza, M.; Marzullo, D.; Bonina, F.; Casteli, F. Flavonoids as antioxidant agents: Importance of their interaction with biomembranes. *Free Radical Biol. Med.* **1995**, *19*, 483−686.
(22) Silva, M. M.; Santos, M. R.; Caroco, G.; Rocha, R.; Justino, G.; Mira, L. Structure-antioxidant activity relationships. *Free Radical Res.* **2002**, *36*, 1219−1227.
(23) van Acker, S. A. B. E.; van Balen, G. P.; van der Berg, D. J.; van der Vijgh, W. J. F. Influence of the iron chelators on the antioxidant activity of flavonoids. *Biochem. Pharmacol.* **1998**, *56*, 935−943.
(24) Mira, L.; Fernandez, M. T.; Santos, M.; Rocha, R.; Florencio, M. H.; Jennings, K. R. Interactions of flavonoids with iron and copper ions. *Free Radical Biol. Med.* **2002**, *36*, 1199−1208.
(25) Pietta, P. G. Flavonoids as antioxidants. *J. Nat. Prod.* **2000**, *63*, 1035−1051.
(26) Lovejoy, D. B.; Richardson, D. R. Iron Chelators as antiproliferative agents. *Curr. Med. Chem.* **2003**, *10*, 1035−1039.
(27) Pan, O.; Kleer, G. G.; Golan, K. L.; Brewer, G. Copper deficiency induced by tetrathiomolybdate suppressing tumor growth and angiogenesis. *Cancer Res.* **2002**, *62*, 4854−4859.
(28) Abeysinghe, R. D.; Greene, B. T.; Haynes, R. The p-53 independent apoptosis mediated by tachpyridine. *Carcinogenesis* **2001**, *22*, 1607−1614.
(29) Fan, O.; Iyer, J.; Zhu, S. Inhibition of N-myc expression and induction of apoptosis by iron chelator, in human neuroblastoma cells. *Cancer Res.* **2001**, *61*, 1073−1079.
(30) Liu, G.Y.; Frank. N.; Bartsch. H.; Lin. J. K. Induction of apoptosis by thuramdisulfides, the reactive metabolites of dithiocarbamates through coordinate modulation of NF-κB, c-fos/c-jun and p-53 proteins. *Mol. Carconog.* **1998**, *22*, 235−246.
(31) von, Angerer E., Keppler, B. K., Eds. *Metal Complexes in Cancer Chemotherapy*; VCH: Weinham, Germany, 1993; pp 73−80.
(32) Fasmon J.; Heinisch G.; Holzer W. Thiosemicarbazone derivatives of pyridazinecarbaldehydes and alkyl pyridazinyl ketones. *Heterocycles* **1989**, *29* 1399−1408.
(33) West, D. X.; Padhye, S. B.; Sonawane, P. B. Structural and physical correlations in the biological properties of transition metal N-heterocyclic thiosemicarbazones. *Struct. Bonding* **1991**, *76*, 1−51.
(34) Nawar, N.; Hosny, N. M. Synthesis, spectral and antimicrobial activity studies of *o*-aminoacetophenone *o*-hydroxybenzoylhydrazone complexes. *Trans. Met. Chem.* **2000**, *25*, 1−8.
(35) Garg, B. S.; Singh, P. K.; Sharma, J. L. Synthesis and characterization of transition metal(II) complexes of salicylaldehyde-2-furoylhydrazone. *Synth. React. Inorg. Met.-Org. Chem.* **2000**, *30*, 803−813.
(36) Sangeetha, N. R.; Pal, S. A family of dinuclear vanadium(V) complexes containing the {OV (μ-O) VO} 4+ core: Syntheses, structures, and properties. *Bull. Chem. Soc. Jpn.* **2000**, *73*, 357−363.
(37) Kong, A. N.; Owuor, E.; Yu, R.; Induction of xenobiotics enzymes by the MAP kinase pathway and the antioxidant or electrophile response element. *Drug Metab. Rev.* **2001**, *33*, 255−271.
(38) Yu, R.; Lei, W.; Madelkar, S.; Weber, M. J.; Der, C. J.; Wu, J.; Kong. A. T. Role of nitrogen activated kinase pathway in the induction of phase detoxifying enzymes by chemicals. *J. Biol. Chem.* **1999**, *274*, 27545−27552.

(39) Hathaway, B. J.; Billing, D. E. Electronic properties and stereochemistries of mononuclear complexes of copper(II) ions. *Coord. Chem. Rev*. **1970**, *5*, 143−207.
(40) Lever, A. B. P. *Inorganic Electronic Spectroscopy*, 2nd ed.; Elsevier: New York, 1984.
(41) West, D. X.; Salberg, M. M.; Bain, G. A.; Liberta, A. E.; Valdes-Martinez, J.; Hernandez-Ortega, S. J. Nickel(II) and copper(II) complexes of 5-substituted formylthiophene thiosemicarbazone. *Transition Met. Chem. (Dordrecht, Neth.)* **1996**, *21*, 206−209.
(42) West, D. X.; Yang, Y.; Klein, T. L.; Goldberg, K. I.; Liberta, A. E.; Valdes-Martinez, J.; Toscano, R. A. Binuclear copper(II) complexes of 2-hydroxyacetophenone N^4-substituted thiosemicarbazones. *Polyhedron* **1995**, *14*, 1681−1693.
(43) Earnshaw, A. *An Introduction to Magnetochemistry*; Academic Press: London, 1968.
(44) Mabbs, F. E.; Machin, D. J. *Magnetism and Transition Metal Complexes*; Chapman and Hall: London, 1973.
(45) Kato, M.; Fanning, J. C.; Jonassen, H. B. Copper complexes of subnormal magnetic moments. *Chem. Rev.* **1969**, *64*, 99−125.
(46) Diaz, A.; Cao, R.; Fargoso, A.; Sanchez, I. Interpretation of SOD-like activity of a series of copper complexes with thiosemicarbazones. *Inorg. Chem. Commun*. **1999**, *2*, 358−360.
(47) Sonawane, P.; Chikate, R.; Kumbhar, A.; Padhye, S.; Doedens, R. J. Inequivalent coordination of thiosemicarbazone ligands in Co(III) and Cr(III) complexes. *Polyhedron* **1994**, *13*, 395−401.
(48) Godlewska, A.; Augustyniak, R.; Bodera, P. Isoflavonoids and their 3′- and 4′-O-substituted derivatives as inhibitors of SH2 domain of $p56^{LCk}$ protein tyrosine kinase. *Cell. Mol. Biol. Lett*. **2005**, *10*, suppl 2.
(49) Milburn, C. C.; Deak, M.; Kelley, S. M.; Price, N. C.; Alessi, D. R.; van Aalten, D. M. F. Biochemistry. binding of phosphatidylinositol 3,4,5-trisphosphate to the pleckstrin homology domain of protein kinase B induces a conformational change. *Biochemistry* **2003**, *375*, 531−538.
(50) *MDS 1.0 Molecular Design Suite*; VLife Sciences Technologies, Pvt Ltd.: Pune, India, 2003.
(51) Yang, J.; Cron, P.; Thompson, V.; Good, V.; Hess, D.; Hemmings, B.; Barford, D. Molecular mechanism for the regulation of protein kinase B/Akt by hydrophobic motif phosphorylation. *Mol. Cell* **2002**, *9*, 1227−1240.
(52) Yang, J.; Cron, P.; Good, V. M.; Thompson, V.; Hemmings, B. A.; Barford, D. Crystal structure of an activated Akt/protein kinase B ternary complex with Gsk-3 peptide and AMP-Pnp. *Nat. Struct. Biol*. **2002** 9, 940−944.
(53) Chang, G.; Guida, W. C.; Still, W. C. An internal coordinate Monte Carlo method for searching conformational space. *J. Am Chem. Soc*. **1989**, *111*, 4379−4386.
(54) Halgren, T. A. Merck molecular force field. V. Extension of MMFF94 using experimental data, additional computational data and empirical rules. *J. Comp. Chem.* **1996**, *17*, 616−641.
(55) Halgren, T. Maximally diagonal force constants in dependent angle-bending coordinates. II. Implications for the design of empirical force fields. *J. Am. Chem. Soc*. **1990**, *112*, 4710−4723.
(56) Padhye, S.B.; Afrasiabi, Z.; Sinn, E.; Fok, J.; Mehta, K.; Rath, N. Antitumor metallothiosemicarbazonates: Structure and antitumor activity of palladium complex of phenanthrequinone thiosemicarbazone. *J. Inorg. Chem.* **2005**, *44*, 1154−1156.
(57) Hill, Z. D.; MacCarthy, P. Novel approach to Job's method. *J. Chem. Educ.* **1986**, *63*, 162−167.
(58) Hathway, B. J. *Comprehensive Coordination Chemistry*, Pergamon Press: London, 1987; vol 5, pp 533−774.
(59) Alessi, D. R.; Caudwell, F. B.; Andjelkovic, M.; Hemmings, B. A.; Cohen, P. Molecular basis for the substrate specificity of protein kinase B; comparison with MAP Kinase 1 and p70 Sb kinase. *FEBS Lett*. **1996**, *399*, 333−338.
(60) Alessi, D. R.; Cohen, P.; Ashworth, A.; Cowley, S.; Leevers, S. J.; Marshall, C. J. Assay and expression of mitogen activated protein kinase, MAP kinase and Raf. *Methods Enzymol*. **1995**, *255*, 279−290.
(61) Kane. L. P.; Shapiro. V. S.; Stokoe. D.; Weiss. A.; Induction of NF-κB by the Akt/PKB kinase. *Curr. Biol*. **1999**, *9*, 601−604.
(62) Reusch, H. P.; Zimmermann, S.; Schaefer, M.; Paul, M.; Moelling, K.; Regulation of Raf by Akt controls growth and differentiation in vascular smooth muscle cells. *J. Biol. Chem*. **2001**, *276*, 33630−33637.
(63) Mohammad, R. M.; Al-Katib, A.; Pettit, G. R.; Vaitkevicius, V. K.; Joshi, U.; Adsay, V.; Majumdar, A. P.; Sarkar, F. H. An orthotopic model of human pancreatic cancer in severe combined immunodeficient mice: Potential application for preclinical studies. *Clin. Cancer Res*. **1998**, *4*, 887−894.
(64) Li, Y.; Bhagat, S.; Ellis, K. L.; Kucuk, O.; Deorge, D. R.; Abrams, J.; Cher, M. L.; Sarkar, F. H. Regulation of gene expression and inhibition of experimental prostate cancer bone metastasis by dietary genistein. *Neoplasia* **2004**, *6*, 354−363.
(65) Hillman, G. G.; Wang, Y.; Kucuk, O.; Che, M.; Doerge, D. R.; Yudelev, M.; Joiner, M. C.; Marples, B.; Forman, J. D.; Sarlar, F. H. Genistein potentiates inhibition of tumor growth by radiation in a prostate cancer orthotopic model. *Mol. Cancer Ther*. **2004**, *30*, 1271−1279.
(66) Banerjee, S.; Zhang, Y.; Ali, S.; Bhuiyan, M.; Wang, Z.; Chaio, P. J.; Philip, P. A.; Abbruzzese, J.; Sarkar, F. H. Molecular Evidence for Increased Antitumor Activity of Gemcitabine by Genistein In vitro and *In* vivo Using an Orthotopic Model of Pancreatic Cancer. *Cancer Research.* **2005**, *65*, 9064−9072.

JM051068Y